Phonon induced rank-2 U(1) nematic liquid states

Han Yan (闫寒)^{1,2,*} and Andriy Nevidomskyy²

¹Rice Academy of Fellows, Rice University, Houston, TX 77005, USA ²Department of Physics & Astronomy, Rice University, Houston, TX 77005, USA (Dated: August 27, 2021)

Fascinating new phases of matter can emerge from strong electron interactions in solids. In recent years, a new exotic class of many-body phases, described by generalized electromagnetism of symmetric rank-2 electric and magnetic fields and immobile charge excitations dubbed fractons, has attracted wide attention. Beside interesting properties in their own right, they are also closely related to gapped fracton quantum orders, new phases of dipole-coversing systems, quantum information, and quantum gravity. However, experimental realization of the rank-2 U(1) gauge theory is still absent, and even known practical experimental routes are scarce. In this work we propose a scheme of coupled optical phonons and nematics as well as several of its concrete experimental constructions. They can realize the electrostatics sector of the rank-2 U(1) gauge theory. A great advantage of our scheme is that it requires only basic ingredients of phonon and nematic physics, hence can be applied to a wide range of nematic matters from liquid crystals to electron orbitals. We expect this work will provide crucial guidance for the realization of rank-2 U(1) and fracton states of matter on a variety of platforms.

"Emergence" – laws of nature arising as the effective theory describing many-body systems – is one of their most fascinating aspects¹, both for intellectual curiosity and practical utility. In the past few decades, tremendous progress has been made in understanding phases beyond the traditional Landau-Ginzburg paradigm of symmetry breaking. One such example are the spin liquids – exotic states built on quantum superposition of product states, characterized not by any order parameter but topological entanglement and topological order. A subclass of such spin liquids can be described by local constraints on the local degrees of freedom (DoF), leading to the emergence of a local gauge invariance, and thereby to topological orders, and exhibit fractionalised excitations and longrange entanglement^{2–5}. A well-known example is quantum spin ice on the pyrochlore lattice, which realizes U(1)gauge theory⁶. It hosts emergent excitations mimicking exactly Maxwell electrodynamics: photons, electric charges and even magnetic monopoles. As such, it has been under intense theoretical³⁻¹⁵ and experimental¹⁶⁻²⁴ investigation.

Recently, a class of more exotic forms of emergent electrodynamics proposed as effective theories for spin

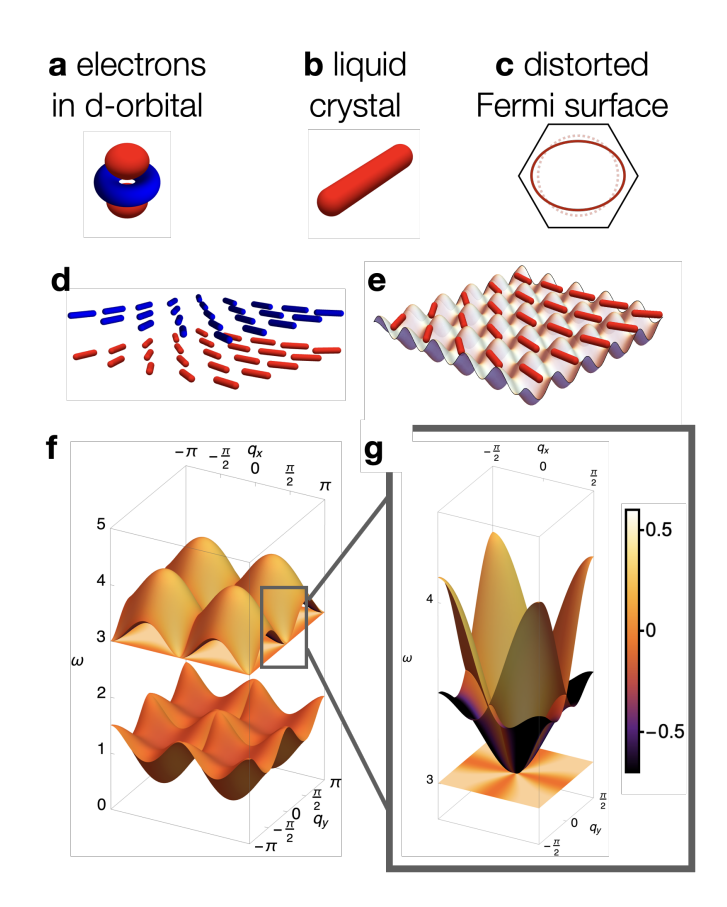


FIG. 1. Realizing rank-2 U(1) electrostatics via optical phonon-nematic coupling. a-c Examples of microscopic objects with nematic degrees of freedom. d Bilayer nematic as a representative experimental construction that realizes the ideal model [Eq. (1)]. e Nematic layer trapped in an artificial periodic potential as a representative experimental construction. f The band structure of [Eq. (1)]. g Zoomed-in view of the phonon-nematic band structure, in which the flat band corresponds to the vector-charge-free nematic configurations, and the upward dispersing bands correspond to the charged nematic configurations.

liquid phases $^{25-28}$ has attracted considerable attention. As a generalization of Maxwell electrodynamics, it features electric and guage fields in the form of rank-2 (R2), or higher-rank, symmetry tensors. The correspondingly modified charge conservation laws result in some unexpected, exciting properties. The electric charge excitations dubbed fractons are intrinsically constrained from moving in the system, and foreshadow a new class of gapped fracton quantum liquid order beyond topological order $^{29-40}$. The rank-2 U(1) (R2-U1) theories

are also shown to be akin to gravity^{25,41–43}, and related to new phases of matter featuring dipole conserving dynamics^{44–48}.

However, these remarkable properties come with cost: the central ingredient – local constraints applied to tensors – is in a more complex form than the traditional Gauss's law of Maxwell electromagnetism. To enforce these constraints, complicated interactions are a necessity in many prototypical fracton models^{25,27,29,31–33,49,50}, while experimental proposals remain scarce ^{37,51,52}. Therefore, concrete design for experimental realization of R2-U1 phases – a crucial step for future development of this field – remains to be a significant challenge.

Results and Discussion

Ingredients for the effective theory. Here we propose a highly generic and realistic experimental scheme to achieve nematic liquid states described by R2-U1 theory. States of matter with nematic DoF, such as liquid crystals, are good potential candidates for this purpose since they are naturally represented by symmetric tensors - exactly those needed in the R2-U1 liquid physics. The challenge is to find a realistic approach toward the specific low-energy Hamiltonian that gives rise to a nematic liquid state obeying the R2-U1 Gauss's law. In this work we show that this is readily achievable. The ingredients in our model are quite common: Einstein phonons and the most general coupling between phonons and nematic DoFs. We demonstrate that integrating out the phonon modes leads precisely to the sought Gauss's law-enforcing term on the remaining nematic DoF. Beside the idealized effective theory, we present a few concrete experimental constructions that can be used to realize such a theory.

Our approach has the advantage of having a wide range of applicability. The existence of nematics at different scales – from electron orbitals to organic molecules, to soft matter – means that our proposed design can be realized in a variety of experimental applications. Different types of nematic matters available also enable us to construct different versions of R2-U1. We hope our work opens a gateway to experimental realizations of R2-U1 theories for a wide spectrum of the physics community.

The idealized model. The ideal model Hamiltonian to realize the R2-U1 physics via nematic-phonon coupling is composed of three parts,

$$\mathcal{H}_{\text{classical}} = \mathcal{H}_{\text{ph}} + \mathcal{H}_{\text{ph-nem}} + \mathcal{H}_{\text{nem}}$$

$$= \frac{\rho \omega_0^2}{2} \boldsymbol{u} \cdot \boldsymbol{u} - \lambda \varepsilon_{ij} \Phi_{ij} + M \sum_{i < i} \Phi_{ij}^2, \qquad (1)$$

where u(r) is the lattice distortion of the Einstein phonons (i.e., phonons with a flat energy dispersion $\hbar\omega_0$). The second term $\mathcal{H}_{\text{ph-nem}}$ is the most natural linear cou-

pling between the strain tensor of the lattice distortion

$$\varepsilon_{ij}(\mathbf{r}) = \partial_i u_j(\mathbf{r}) + \partial_j u_i(\mathbf{r}),$$
 (2)

and the nematic DoF described by the symmetric tensor Φ_{ij}^{53-57} . The third term \mathcal{H}_{nem} is a simple on-site potential (mass term) for the nematics. Often the nematics are constrained by a "unit-tensor"-like condition $\sum_{i\leq j}\Phi_{ij}^2=1$ (see section **Discussion** on their microscopic origins), so the third term can be dropped as long as the constraint is taken into account properly. Finally, in this Hamiltonian we have suppressed the dynamical term

$$\mathcal{H}_{\text{dynamics}} = (\partial_t \boldsymbol{u})^2 + (\partial_t \boldsymbol{\Phi})^2, \tag{3}$$

since we are mostly interested in the classical sector of the system. Their potential role in a quantum system is also discussed in the section **Discussion**.

The spectrum of the diagonized Hamiltonian on a square lattice is shown on Fig. 1(f,g) (see Fig. 5 for the square lattice set up). The spectrum intensity distribution on each band is measured by $\langle \Phi_{xx}(-q)\Phi_{yy}(q)\rangle$, whose meaning will be clarified in a later part of this section.

By integrating out the Gaussian phonon modes, we end up with the effective theory for the nematic DoF only, described by the Hamiltonian

$$\mathcal{H}_{\text{nem-eff}} = \Lambda(\partial_i \Phi_{ij})(\partial_k \Phi_{kj}) + M \sum_{i < j} \Phi_{ij}^2, \qquad (4)$$

where $\Lambda = \lambda^2/(2\rho\omega_0^2)$. In the limit of sufficiently large $\Lambda \gg T$ relative to the temperature, the first term imposes high energy cost for Φ_{ij} configurations that violate the constraint

$$\partial_i \Phi_{ij} = 0. (5)$$

Upon identifying the nematic DoF with the generalized rank-2 electric field E_{ij} :

$$\Phi \longleftrightarrow E, \quad \partial_i \Phi_{ij} \longleftrightarrow \rho_i \equiv \partial_i E_{ij},$$
 (6)

Eq. (5) becomes exactly the Gauss's law for the vectorcharged R2-U1 theory. Hence the classical R2-U1 nematic liquid state is realized in the low energy sector of the theory.

A more physical interpretation of the model is achieved by noticing that

$$-\lambda \epsilon_{ij} \Phi_{ij} = 2\lambda \boldsymbol{u} \cdot \boldsymbol{\rho} + \text{total derivative.}$$
 (7)

This means the vector charge excitation ρ is linearly coupled to the lattice distortion. The energy cost of the lattice distortion induces, upon integrating out the lattice DoF, the potential energy $\lambda^2 \rho^2/(2\rho\omega_0^2)$ for the charge excitations

To quantitatively show the emergence of R2-U1 electrostatics, we study the model of Eq. (4) on a square lattice under the on-site constraint $\sum_{i \leq j} \Phi_{ij}(r)^2 = 1$ and

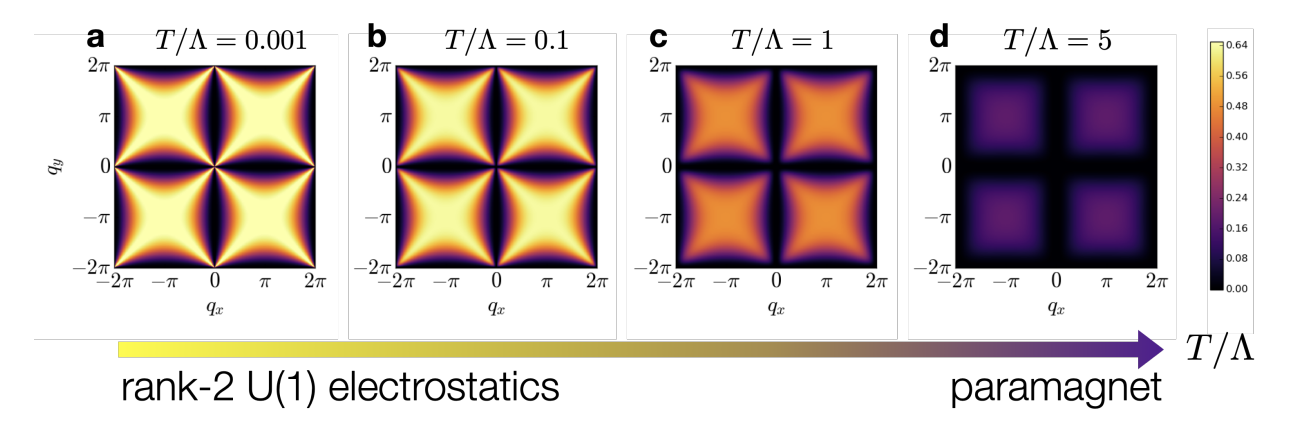


FIG. 2. Nematic correlation functions $\langle \Phi_{xx}(-q)\Phi_{yy}(q)\rangle$ for model in Eq. (4). The four panels show the correlation functions, using a false-color map, computed via the Self-Consistent Gaussian Approximation (see Methods) on a square lattice [Fig. 5] at different temperatures relative to the parameter Λ . The high temperature regime shown in **d** is a paramagnetic phase with vanishing correlations. The low temperature regime shown in **a** is the rank-2 U(1) phase, manifested by the characteristic 4-fold pinch point pattern in the correlation function around q = 0, originating from the functional form $\langle \Phi_{xx}(-q)\Phi_{yy}(q)\rangle \propto q_x^2 q_y^2/q^4$. **b,c** The 4-fold pinch points become gradually smeared due to thermal fluctuations at intermediate temperatures.

examine its correlation function $\langle \Phi_{ij}(-q)\Phi_{kl}(q)\rangle$ at different temperatures using the Self-Consistent Gaussian Approximation (SCGA, described in Methods).

The equal time correlation function $\langle \Phi_{ij}(-\mathbf{q})\Phi_{kl}(\mathbf{q})\rangle$ in the R2-U1 phase is constrained by the Gauss's law $q_{\alpha}\langle \Phi_{ij}(-\mathbf{q})\Phi_{kl}(\mathbf{q})\rangle = 0$, where α is one of the four indices i, j, k, l and, the repeated index is summed over. As a consequence the correlation is restricted to be proportional to a highly anisotropic projector in the form of

$$\langle \Phi_{ij}(-\mathbf{q})\Phi_{kl}(\mathbf{q})\rangle \propto \frac{1}{2} \left(\delta_{ik}\delta_{jl} + \delta_{il}\delta_{jk}\right) + \frac{q_iq_jq_kq_l}{q^4}$$

$$-\frac{1}{2} \left(\delta_{ik}\frac{q_jq_l}{q^2} + \delta_{jk}\frac{q_iq_l}{q^2} + \delta_{il}\frac{q_jq_k}{q^2} + \delta_{jl}\frac{q_iq_k}{q^2}\right).$$
(8)

In particular, $\langle \Phi_{xx}(-\boldsymbol{q})\Phi_{yy}(\boldsymbol{q})\rangle \propto q_x^2q_y^2/q^4$ shows a characteristic pattern dubbed "4-fold pinch point" ^{58–60}.

In Fig. 2, we present the correlation function $\langle \Phi_{xx}(-q)\Phi_{yy}(q)\rangle$, computed within the SCGA approach, at different ratios of T/Λ . As the result demonstrates, at high temperature, the system is a paramagnet and the correlation function is essentially vanishing. At low temperatures on the other hand, the 4-fold pinch point emerges as the system enters the R2-U1 phase. The transition between the two phases is expected to be not a phase transition but a crossover.

The same 4-fold pinch point is also visible in the band structure of the diagonlized Hamiltonian shown in Fig. 1(f,g). There, the flat band corresponds to the nematic states obeying Gauss's law. Note that the energy of this flat band is finite due to the non-zero mass M in Eq. (4), and the lack of dispersion is due to the fact that the mass term imposes a local constraint, i.e. all such states are momentum independent. The 4-fold

pinch point is imprinted on the flat band, which is consistent with the result from the Gaussian-integrated theory [Eq. (4)].

Advantages and challenges of the idealized model. Some comments are in order before we go on to discuss more concrete experimental set-ups to realize the ideal Hamiltonian. First, this model has the advantage of being built upon most common elements in phonon and nematic physics. The Einstein phonon is the zerodispersion limit of optical phonon, which is often a good approximation. More generally, optical phonons with small dispersions also work, since mild dispersion only contributes to the higher-order terms. The nematics DoF are common microscopic objects, ranging in their origin from molecular anisotropy in classical liquid crystals, to orbital electron DoF in transition-metal compounds [cf. Fig. 1(a-c) and **Discussion**]. The tendency towards the nematic distortion can also be emergent, for instance due to the Pomeranchuk instability of a Fermi surface⁶¹. The phonon-nematic coupling in the second term of Eq. (1) is the lowest order coupling that respects the rotational symmetry of the system and is also generally expected, as seen in many other studies 53-57. Hence we expect it to be the dominant term in many experiments.

The remaining challenge of realizing Eq. (1) is that while all three elements are common in experiments, the phonon-nematic coupling $\mathcal{H}_{\rm ph-nem}$ is usually for acoustic phonons, while the ones needed here are optical. The consequence of acoustic phonons coupled to nematics has been discussed in detail in Refs. ^{55–57}. There, although the coupling also yields a 4-fold-symmetric anisotropy similar to those shown in Fig. 2, the resulting effective theory is not of the form of the sought-after rank-2 U(1) electromagnetism. The reason for demanding a finite (albeit possibly small) energy ω_0 of optical phonons is to

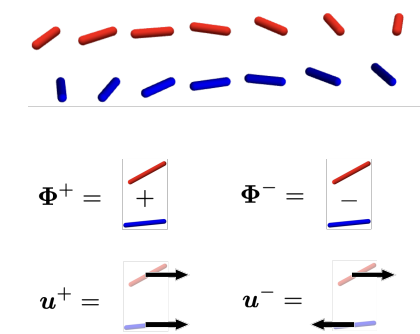


FIG. 3. A bilayer construction of two lattices with nematic degrees of freedom. The atomic lattices are not shown for clarity but are essential in hosting intra-layer acoustic phonons. The inter-layer coupling results in the phonon splitting into two sectors: the acoustic in-phase mode (u^+) and the optical out-of-phase mode (u^-) in Eq. (11). These two phonon modes couple to the corresponding nematic DoFs $(\Psi^+$ and $\Psi^-)$ in the appropriate sectors. It is the coupling in the out-of-phase optical sector in Eq. (12) that leads to the rank-2 U(1) theory.

ensure that integrating out these higher-energy DoF is legitimate, leading to a finite $\Lambda \equiv \lambda^2/(2\rho\omega_0^2)$ in Eq. (4).

In what follows we discuss concrete experimental setups that resolve the main challenge: how to implement the desired coupling between the nematic and opticalphonon DoF.

Proposal 1: Bilayer construction. For two-dimensional systems, one solution we propose is to construct systems with multiple sublattice sites. Here we consider an example of coupling two layers together, with each hosting the common acoustic phonon-nematic coupling [Fig. 1(d)].

Each single layer, in the most symmetric case, is described by the Hamiltonian

$$\mathcal{H}_{\text{ac-ph-nem}} = 2\rho v^2 (\partial_i u_j^X) (\partial_i u_j^X) - \lambda \varepsilon_{ij}^X \Phi_{ij}^X + M \sum_{i \le j} (\Phi_{ij}^X)^2. \tag{9}$$

Here $X=\mathrm{T},\mathrm{B}$ corresponds to the top and bottom layer, and the acoustic phonon modes have isotropic linear dispersion $\omega_{ac}=vq$ (again here the dynamical terms are omitted).

We then consider the two layers coupled by the following interaction:

$$\mathcal{H}_{\text{int}} = g\rho(\mathbf{u}^{\text{T}} - \mathbf{u}^{\text{B}})^{2}. \tag{10}$$

Such interaction appears naturally from an inter-atomic potential for the lattice sites penalizing their deviation from the equilibrium positions, due to the attraction/repulsion between the two layers.

Diagonalizing $\mathcal{H}_{ac\text{-ph-nem}} + \mathcal{H}_{int}$, we find that the DoF can be decomposed into the in-phase and out-of-phase

sectors labeled by +, - [cf. Fig. 3],

$$u^{\pm} = \frac{1}{\sqrt{2}} (u^{\mathrm{T}} \pm u^{\mathrm{B}}),$$

$$\Phi^{\pm} = \frac{1}{\sqrt{2}} (\Phi^{\mathrm{T}} \pm \Phi^{\mathrm{B}}).$$
(11)

The two sectors decouple from each other. The "+" sector is described again by the usual acoustic phonon-nematic coupling as in Eq. (9), and hence is not of our interest. The out-of-phase "-" sector describes the inter-layer optical phonon, coupled to the corresponding inter-layer nematic DoF:

$$\mathcal{H}_{-} = 2\rho v^{2} \sum_{i} (\nabla u_{i}^{-})^{2} + 2g\rho u^{-} \cdot u^{-} - \lambda \varepsilon_{ij}^{-} \Phi_{ij}^{-} + M \sum_{i \leq j} \Phi_{ij}^{-2}.$$
(12)

Here, the phonons associated with u^- becomes gapped because of the inter-layer coupling [Eq. (10)]. The last three terms in Eq. (12) are exactly what we are after. The first term induces the dispersion to the inter-layer optical phonon. Integrating out the photons, this term yields an additional, **q**-depenent contribution of the order of $\mathcal{O}\left(\frac{\lambda^2 v^2 q^4}{\rho g^2}(\mathbf{\Phi})^2\right)$. This is to be compared to the principal term in the Gauss's law, of the order of $\mathcal{O}\left(\frac{\lambda^2 q^2}{\rho g}(\mathbf{\Phi})^2\right)$. Hence, if the dispersion scale is small compare to the gap, i.e., $vq_0^2 \ll g \ (q_0 \sim 1/a \ \text{denoting}$ the edge of the Brillouin zone), then the phonon bands will be sufficiently flat, and we obtain the idealized model of Eq. (1) to a good approximation, with $\Lambda = \frac{\lambda^2}{\rho q}$.

Proposal 2: Mutliple sublattice sites. The essence of the proposal in the previous section is that, when there are multiple sublattice sites in the system, the total number of phonon branches increases accordingly, yet only one set of acoustic phonons exists, and the remaining phonon branches will become gapped, as desired to obtain the idealized model in Eq. (1). Similar approaches can be designed following this principle. For example, a single-layer nematic lattice with two sub-lattice sites per unit cell can also work [Fig. 4(a)].

Proposal 3: Artificial potential well. Another scheme we propose is to introduce an artificial potential for the nematic-site lattice displacements, in order to gap the phonons directly. That is, we add a potential term

$$\mathcal{H}_{\text{pot}} = \frac{\rho \omega_0^2}{2} \boldsymbol{u} \cdot \boldsymbol{u} \tag{13}$$

to the lattice distortion, thus approximating the idealized model in Eq. (1) when the phonon dispersion is mild.

The first realization of this idea is schematically illustrated in Fig. 1(e), wherein the nematic atoms/molecules are placed in a periodic optical (laser) potential. Such periodic potential is a sophisticated experimental technique in use already $^{62-69}$.

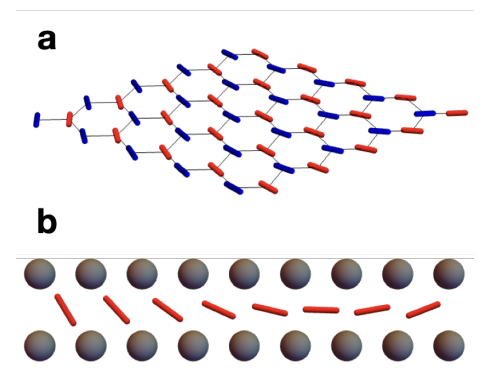


FIG. 4. Proposed experimental setups to realize the ideal model of Eq. (1). a The multiple sublattice site construction. Shown as an example is a hexagon lattice of nematic degrees of freedom residing on two sublattice sites (blue and red rods). b The artificial potential well construction. The nematic layer (red rods) is sandwiched between two substrates of heavy molecules (grey balls). The substrates serve as sources of the artificial potential term [Eq. (13)] for the lattice distortion u in the nematic layer.

Another possible realization is to sandwich the nematic layer between the substrate layers of heavy molecules. The latter would then introduce a potential term to the nematics layer, as illustrated in Fig. 4(b). **Discussion:**

beyond the classical model. In this work we focused on how to achieve the electrostatics sector of the rank-2 U(1) theory, which is purely classical. This is one of the most crucial steps toward the quantum electrodynamics of R2-U1, just as how a classical spin ice provides the underpinnings for the development of a quantum spin ice.

Nevertheless, let us now discuss how quantum dynamics can arise in our model, which will render it the full-fledged rank-2 electrodynamics. We start with a concrete example, and then discuss the general principles applicable to all the implementations proposed above .

For concreteness, let us consider Φ living on the square lattice. For better visualization, we place the Φ_{xx} , Φ_{yy} components on the vertices, and shift $\Phi_{xy} = \Phi_{yx}$ to the centers of the plaquettes. This is illustrated in Fig. 5(a,b). The generalized vector charges $\vec{\rho} = (\rho_x, \rho_y)$ are then defined on the links of the lattice. Specifically, ρ_x is defined on the x-oriented links as $\rho_x = \Delta_x \Phi_{xx} + \Delta_y \Phi_{yx}$, where Δ_i is the lattice derivative. Similarly ρ_y is defined on y-links as $\rho_y = \Delta_y \Phi_{yy} + \Delta_x \Phi_{xy}$. The classical sector of the Hamiltonian is

$$\mathcal{H}_{\text{sq-cl}} = U \boldsymbol{\rho}^2 + M \sum_{i \le j} \Phi_{ij}^2.$$
 (14)

To introduce quantum dynamics, we assume that each component of Φ corresponds to the S^z of a quantum spin with large spin number, and there is a generalized

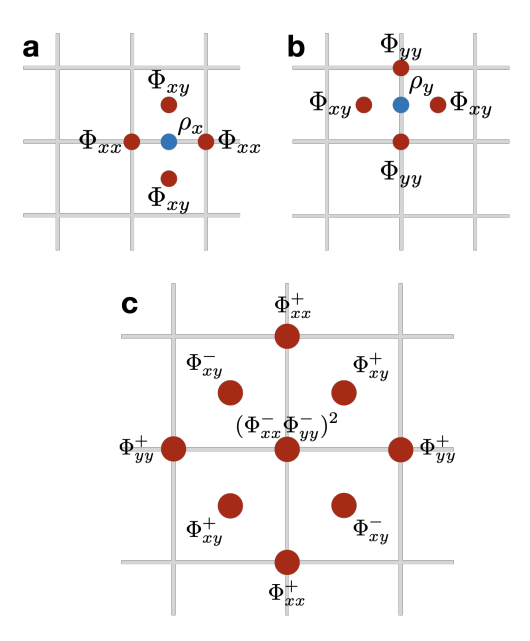


FIG. 5. The square lattice model of the nematic degrees of freedom. This model is used for computing the correlation functions in Eq. (8) and throughout the paper. a, b Nematic degrees of freedom Φ_{xx} and Φ_{yy} defined on the vertices of the lattice, with off-diagonal components Φ_{xy} situated in the centers of the plaquettes. The lattice representation of the vector charge ρ in Eq. (6) has two components $\rho = (\rho_x, \rho_y)$ which live on the x- and y-links of the lattice, respectively, based on the four Φ_{ij} surrounding it. c A dynamical term that acts as the gauge-invariant magnetic field in the generalized rank-2 electrodynamics. This term is a product of twelve ϕ_{ij}^{\pm} operators shown. When acting on a Gauss's law-obeying charge-free electric field configuration, the state is mapped onto another charge-free configuration.

"transverse field" applied to the nematic DoFs,

$$\mathcal{H}_{\text{sq-dy}} = h \sum_{i \le j} (\Phi_{ij}^+ + \Phi_{ij}^-), \tag{15}$$

where Φ_{ij}^{\pm} are the raising and lowering operators of Φ_{ij} . Crudely speaking, Φ_{ij}^{\pm} plays the role of the gauge field operator \boldsymbol{A} associated with the charge creation terms, since they are canonically conjugate to the electric field components \boldsymbol{E} , and creates charges when applied to a Φ_{ii} .

A single operation of Φ_{xx}^{\pm} or Φ_{yy}^{\pm} will create charges in the system. Within the sub-Hilbert space of the Gauss's law obeying states, operators Φ_{ij}^{\pm} can only act on the Hilbert space at a higher perturbative order, such as to cancel all the charges created. An example we denote as Φ_{comp}^{+} is shown in Fig. 5(c). There, a specific product of twelve ϕ_{ij}^{\pm} operators maps one charge-free electric field configuration to another. The fact that no charge is created anywhere in the system is equivalent to that this composite product of these 12 operators is gauge invariant – that is, Φ_{comp}^{+} (and also $\Phi_{\text{comp}}^{-} \equiv (\Phi_{\text{comp}}^{+})^{\dagger}$) plays the role of the generalized magnetic field of R2-U1 theory.

The electrodynamics is realized by the Hamiltonian

$$\mathcal{H}_{\text{sq-full}} = U \rho^2 + M \sum_{i < j} \Phi_{ij}^2 + \mu (\Phi_{\text{comp}}^- + \Phi_{\text{comp}}^+).$$
 (16)

Now let us comment on the general properties of the quantum dynamics of the nematic R2-U1 theory. Like in a quantum spin ice, the emergent magnetic field usually involves multiple operators, and is generated perturbatively via the product of transverse field operators which preserve the Gauss's law. In a quantum spin ice, or lattice scalar-U(1) theory in general, these composite operators are simply loops of the dynamical operators, forming a lattice realization of the magnetic flux $\oint \nabla \times \mathbf{A} \, \mathrm{d}l = \iint \mathbf{B} \, \mathrm{d}\sigma$. In R2-U1 theory, the composite operators become more complicated as shown in the square lattice example above.

Although the long-wave length theory will remain the same, on different lattice models the available quantum dynamical terms will depend on the details of the lattice and the microscopic implementation of the nematic DoF. It is also possible that the quantum dynamics leads the system into other phases instead of R2-U1 electrodynamics. How the generalized magnetic field arises, if it can be realized in the first place, will have to be discussed on a case-by-case basis.

Discussion: Microscopic origin of the nematics. In our construction, we tacitly assumed that the nematic DoF are described by a symmetric tensor with all its independent components, of which there are 3 in two-dimensional systems and 5 in three-dimensional. Depending on the microscopic origin of the nematics, the number of DoF in the symmetric tensor representation may be fewer than those numbers. Below, we provide several concrete examples of the various microscopic realizations of the nematic DoFs.

The first example is that of d-electrons in transition metals (Fig. 1(a)). There are in total five such orbitals corresponding to the $|l=2; m=-2,-1,\ldots,2\rangle$ states in the spherical harmonic expansion. They form a symmetric, traceless tensor representation of the group SU(2) describing rotations in the orbital Hilbert space (the l=0,1representations are the trace and anti-symmetric components of this matrix). Ignoring the crystal field effects, which generically lift the orbital SU(2) symmetry, these five orbitals form a degenerate manifold, out of which an orbital-nematic order can appear if the symmetry is spontaneously broken. In the disordered, symmetrypreserving phase, these orbital degrees of freedom can be used to construct classical rank-2 electrostatics as outlined in this work. Moreover, by virtue of being intrinsically quantum objects, such models are also good candidates for constructing quantum electrodynamics of R2-U1 theory.

The second example of the nematics is a classical liquid crystal. In 2D, such as shown schematically in Fig. 1(b), the nematicity is described by a director of a fixed length,

encoded in a 2×2 symmetric matrix

$$\mathbf{\Phi} = \begin{pmatrix} \cos 2\theta & \sin 2\theta \\ \sin 2\theta & -\cos 2\theta \end{pmatrix}. \tag{17}$$

Note that the matrix is traceless and unimodular (reflecting the fact that director is of unit length), and as a result, nematic DoF are described by a single independent parameter, the azimuthal angle θ . The idealized theory presented in the beginning still holds, however the constraints on the nematic matrix mean that the resulting phase may be modified.

Another example of the nematicity is the spontaneous distortion of the Fermi surface (see e.g. Fig. 1(c)), known as the Pomeranchuk instability⁶¹, which in the simplest case of an isotropic (circular in 2D) Fermi surface is described by the quadrupole density operator (see e.g. Ref. 70)

$$\mathbf{\Phi}_{FS}(\mathbf{q}) = \frac{1}{k_F^2} \psi^{\dagger}(\mathbf{q}) \begin{pmatrix} q_x^2 - q_y^2 & q_x q_y \\ q_x q_y & q_y^2 - q_x^2 \end{pmatrix} \psi(\mathbf{q}), \quad (18)$$

where $\psi^{\dagger}(\boldsymbol{q})$ and $\psi(\boldsymbol{q})$ are the electron creation/annihilation operators at momentum \boldsymbol{q} . The above matrix is also traceless, yielding traceless R2-U1 theory upon integration of the phonon modes coupled to Φ_{FS} as in Eq. (1). The elliptic Fermi surface distortion thus has two independent DoFs: Φ_{xx} and Φ_{xy} , which can also be cast in the form of a complex order parameter $Qe^{i2\theta} = \Phi_{xx} + i\Phi_{xy}$, with the amplitude Q proportional to the eccentricity of the ellipse and angle $\pm\theta$ its azimuthal direction.

We note that in the above example, the presence of the underlying crystalline lattice can pin the Fermi surface distortion along particular direction(s), such as shown in Fig. 1(c). For instance, pinning to $\pm x$ or $\pm y$ directions on the square lattice introduces a potential $U_{lat}(\theta) = -U_0\cos(2\theta)$ for the azimuthal angle. The resulting rank-2 theory would then become discrete, described by a 4-state Potts model on a square lattice (rather than the continuous U(1) parameter). Nevertheless, for temperatures and energy scales above U_0 , the classical theory could be approximately considered to be U(1).

Our final example of the (discrete) nematic order is realized on crystalline lattices with n-fold irreducible representations (n=2,3) of the point group. For instance, hexagonal systems (with point groups C_6 and D_6 in 2D) allow two-dimensional irreducible representations and hence the nematic order parameter can be parametrized by $\Phi = \Phi_0(\cos(2\theta), \sin(2\theta))$, which can be cast in the form of a traceless rank-2 tensor as in Eq. (17). This well known fact has been exploited recently in the discussion of nematicity in the twisted bilayer graphene, where coupling to acoustic phonons (different from the optical phonons in our case) was also considered⁵⁷. Generically, the lattice pinning will result in a four-state Potts model description of the nematic

DoF, analogous to the previous case, and upon integrating out the (optical) phonons, the resulting rank-2 theory will be a discrete one.

When designing possible experimental realizations of the nematic-phonon coupling, one should thus be aware of the consequence of such discretization and the decreased number of the DoF (as exemplified by the traceless condition in example 2 and 3 above), since too few DoF may result in ordered phases or states with subsystem symmetries only. This however could also be a blessing in disguise, since it means we have a wider range of R2–U1 theories accessible in experiment. A particularly interesting type of such theories, for instance, is built in 3D from tensors with all diagonal components vanishing. Such "hollow" rank-2 theories turn out to be the gateways toward gapped fracton order uppon higgsing 34,35, with a great potential for applications in quantum memory storage.

In summary, we presented a theoretical model with simple ingredients that can realize the emergent rank-2 U(1) electrostatics via optical phonon-nematic coupling. Given the intimate connection between this rank-2 generalized electrodynamics and the exotic fracton phases of matter^{26,28}, which have recently garnered much attention, the present work thus paves the way towards natural implementations of the fracton matter in the experiment. Given the simplicity of the ingredients (optical phonons and nematic DoF), we hope this proposal may be realized in various settings, from liquid crystals to bilayer systems, to polar molecules in a periodic optical potential, and we have outlined several such possible constructions. The present proposal yields a classical rank-2 theory, which is a necessary first step on the path towards truly quantum rank-2 electrodynamics and fracton physics. We have outlined a possible route towards such quantum theory by incorporating the generalized magnetic fields into our nematic model.

Methods

Self-consistent Gaussian Approximation. The Self-Consistent Gaussian Approximation (SCGA) is an analytical method that treats the nematics in the large-N limit, which is known to produce rather accurate results in the spin/nematic liquid phases. Our calculation fol-

lows closely the exposition in Ref. 71. We first treat Φ_{ij} as independent, freely fluctuating DoF. The Hamiltonian in the momentum space is written as

$$\mathcal{E}_{\text{Large-}N} = \frac{1}{2}\tilde{\mathbf{\Phi}}\mathcal{H}_{\text{Large-}N}\tilde{\mathbf{\Phi}}^T, \tag{19}$$

written in terms of the triad of nematic components (for the two-dimenstional model) $\tilde{\Phi} = (\Phi_{xx}, \Phi_{yy}, \Phi_{xy})$. The matrix $H_{\text{Large}-N}$ is the Fourier transformed interaction matrix from Eq. (4):

$$H_{\text{Large-}N} = 2\Lambda \begin{pmatrix} C_x^2 & 0 & C_x C_y \\ 0 & C_y^2 & C_x C_y \\ C_x C_y & C_x C_y & C_x^2 + C_y^2 \end{pmatrix}, \qquad (20)$$

where C_x and C_y are the momentum dependent functions. For the square lattice model [Fig. 5], $C_x = 2\sin(q_x/2)$, $C_y = 2\sin(q_y/2)$, with the lattice constant set to 1.

We then introduce a Lagrange multiplier with coefficient $\mu(\beta)$ to the partition function to obtain

$$\mathcal{Z} = \exp\left(-\frac{1}{2}\int_{\mathrm{BZ}} \mathrm{d}\boldsymbol{q} \int \mathrm{d}\tilde{\boldsymbol{\Phi}}\tilde{\boldsymbol{\Phi}} \left[\beta \mathcal{H}_{\mathrm{Large-}N} + \mu(\beta)\mathcal{I}\right]\tilde{\boldsymbol{\Phi}}^{T}\right),\tag{21}$$

where β denotes the inverse temperature. The purpose of the term $\mu(\beta)\tilde{\Phi}\mathcal{I}\tilde{\Phi}^T$ (\mathcal{I} stands for the identity matrix) is to impose, on average, an additional unimodular constraint on the nematic DoF, such that

$$\langle \Phi_{xx}^2 + \Phi_{yy}^2 + \Phi_{xy}^2 \rangle = 1. \tag{22}$$

For a given temperature $T=1/\beta$, the value of $\mu(\beta)$ is numerically obtained by searching for its value that must satisfy the constraint

$$\int_{BZ} d\mathbf{q} \sum_{i=1}^{3} \frac{1}{\lambda_i(\mathbf{q}) + \mu(\beta)} = \langle \Phi_{xx}^2 + \Phi_{yy}^2 + \Phi_{xy}^2 \rangle = 1, (23)$$

where $\lambda_i(\mathbf{q})$, i=1,2,3 are the three eigenvalues of $\beta \mathcal{H}_{\text{Large-}N}(\mathbf{q})$.

With μ fixed, the partition function is completely determined for a free theory of $\tilde{\Phi}$, and all correlation functions in Fig. 2 can be computed from extracting the corresponding components in $[\beta \mathcal{H}_{\text{Large-N}} + \mu(\beta)\mathcal{I}]^{-1}$.

^{*} hy41@rice.edu

Anderson, P. W. More Is Different. Science 177, 393-396 (1972). URL http://science.sciencemag.org/content/

Anderson, P. Resonating valence bonds: A new kind of insulator? Materials Research Bulletin 8, 153-160 (1973). URL http://www.sciencedirect.com/science/article/ pii/0025540873901670.

³ Balents, L. Spin liquids in frustrated magnets. *Nature (London)* **464**, 199-208 (2010). URL http://dx.doi.org/10.1038/nature08917.

⁴ Savary, L. & Balents, L. Quantum spin liquids: a review. Reports on Progress in Physics 80, 016502 (2017). URL http://stacks.iop.org/0034-4885/80/i=1/a=016502.

⁵ Zhou, Y., Kanoda, K. & Ng, T.-K. Quantum spin liquid states. Rev. Mod. Phys. 89, 025003 (2017). URL https:

- //link.aps.org/doi/10.1103/RevModPhys.89.025003.
- ⁶ Hermele, M., Fisher, M. P. A. & Balents, L. Pyrochlore photons: The U(1) spin liquid in a S=½ three-dimensional frustrated magnet. *Phys. Rev. B* **69**, 064404 (2004). URL http://link.aps.org/doi/10.1103/PhysRevB.69.064404.
- Banerjee, A., Isakov, S. V., Damle, K. & Kim, Y. B. Unusual Liquid State of Hard-Core Bosons on the Pyrochlore Lattice. *Phys. Rev. Lett.* **100**, 047208 (2008). URL http://link.aps.org/doi/10.1103/PhysRevLett.100.047208.
- ⁸ Benton, O., Sikora, O. & Shannon, N. Seeing the light: Experimental signatures of emergent electromagnetism in a quantum spin ice. *Phys. Rev. B* **86**, 075154 (2012). URL https://journals.aps.org/prb/abstract/10.1103/PhysRevB.86.075154.
- ⁹ Savary, L. & Balents, L. Coulombic Quantum Liquids in Spin-1/2 Pyrochlores. *Phys. Rev. Lett.* 108, 037202 (2012). URL https://link.aps.org/doi/10.1103/PhysRevLett. 108.037202.
- ¹⁰ Shannon, N., Sikora, O., Pollmann, F., Penc, K. & Fulde, P. Quantum Ice: A Quantum Monte Carlo Study. *Phys. Rev. Lett.* **108**, 067204 (2012). URL https://link.aps.org/doi/10.1103/PhysRevLett.108.067204.
- Hao, Z., Day, A. G. R. & Gingras, M. J. P. Bosonic many-body theory of quantum spin ice. *Phys. Rev. B* 90, 214430 (2014). URL https://link.aps.org/doi/10.1103/PhysRevB.90.214430.
- Gingras, M. J. P. & McClarty, P. A. Quantum spin ice: a search for gapless quantum spin liquids in pyrochlore magnets. *Reports on Progress in Physics* **77**, 056501 (2014). URL http://stacks.iop.org/0034-4885/77/i= 5/a=056501.
- ¹³ Kato, Y. & Onoda, S. Numerical Evidence of Quantum Melting of Spin Ice: Quantum-to-Classical Crossover. Phys. Rev. Lett. 115, 077202 (2015). URL https://link.aps.org/doi/10.1103/PhysRevLett.115.077202.
- Chen, G. Dirac's "magnetic monopoles" in pyrochlore ice U(1) spin liquids: Spectrum and classification. Phys. Rev. B 96, 195127 (2017). URL https://link.aps.org/doi/ 10.1103/PhysRevB.96.195127.
- Huang, C.-J., Deng, Y., Wan, Y. & Meng, Z. Y. Dynamics of Topological Excitations in a Model Quantum Spin Ice. Phys. Rev. Lett. 120, 167202 (2018). URL https://link. aps.org/doi/10.1103/PhysRevLett.120.167202.
- ¹⁶ Zhou, H. D. et al. Dynamic Spin Ice: Pr₂Sn₂O₇. Phys. Rev. Lett. **101**, 227204 (2008). URL https://link.aps.org/doi/10.1103/PhysRevLett.101.227204.
- ¹⁷ Ross, K. A., Savary, L., Gaulin, B. D. & Balents, L. Quantum Excitations in Quantum Spin Ice. *Phys. Rev.* X 1, 021002 (2011). URL https://link.aps.org/doi/10.1103/PhysRevX.1.021002.
- ¹⁸ Fennell, T., Kenzelmann, M., Roessli, B., Haas, M. K. & Cava, R. J. Power-Law Spin Correlations in the Pyrochlore Antiferromagnet Tb₂Ti₂O₇. Phys. Rev. Lett. **109**, 017201 (2012). URL https://link.aps.org/doi/10.1103/PhysRevLett.109.017201.
- 19 Kimura, K. et al. Quantum fluctuations in spin-ice-like Pr₂Zr₂O₇. Nature Communications 4, 1934 (2013). URL http://dx.doi.org/10.1038/ncomms2914http://10.0.4.14/ncomms2914https://www.nature.com/articles/ncomms2914{#}supplementary-information.
- Sibille, R. et al. Candidate Quantum Spin Liquid in the Ce³⁺ Pyrochlore Stannate Ce₂Sn₂O₇. Phys. Rev. Lett. 115, 097202 (2015). URL https://link.aps.org/doi/

- 10.1103/PhysRevLett.115.097202.
- Wen, J.-J. et al. Disordered Route to the Coulomb Quantum Spin Liquid: Random Transverse Fields on Spin Ice in Pr₂Zr₂O₇. Phys. Rev. Lett. 118, 107206 (2017). URL https://link.aps.org/doi/10.1103/PhysRevLett. 118.107206.
- Thompson, J. D. et al. Quasiparticle Breakdown and Spin Hamiltonian of the Frustrated Quantum Pyrochlore Yb₂Ti₂O₇ in a Magnetic Field. Phys. Rev. Lett. 119, 057203 (2017). URL https://link.aps.org/doi/10. 1103/PhysRevLett.119.057203.
- ²³ Sibille, R. et al. Experimental signatures of emergent quantum electrodynamics in Pr2Hf2O7. Nature Physics 14, 711715 (2018). URL https://doi.org/10.1038/s41567-018-0116-x.
- ²⁴ Gao, B. et al. Experimental signatures of a three-dimensional quantum spin liquid in effective spin-1/2 Ce2Zr2O7 pyrochlore. Nature Physics 15, 1052–1057 (2019). URL https://doi.org/10.1038/s41567-019-0577-6.
- ²⁵ Xu, C. Gapless bosonic excitation without symmetry breaking: An algebraic spin liquid with soft gravitons. *Phys. Rev. B* **74**, 224433 (2006). URL https://link.aps. org/doi/10.1103/PhysRevB.74.224433.
- Pretko, M. Generalized electromagnetism of subdimensional particles: A spin liquid story. *Phys. Rev. B* 96, 035119 (2017). URL https://link.aps.org/doi/10.1103/PhysRevB.96.035119.
- Rasmussen, A., You, Y.-Z. & Xu, C. Stable Gapless Bose Liquid Phases without any Symmetry. arXiv e-prints arXiv:1601.08235 (2016).
- Pretko, M. Subdimensional particle structure of higher rank U(1) spin liquids. Phys. Rev. B 95, 115139 (2017). URL https://link.aps.org/doi/10.1103/PhysRevB.95. 115139.
- ²⁹ Chamon, C. Quantum Glassiness in Strongly Correlated Clean Systems: An Example of Topological Overprotection. *Phys. Rev. Lett.* **94**, 040402 (2005). URL https: //link.aps.org/doi/10.1103/PhysRevLett.94.040402.
- ³⁰ Shannon, N., Misguich, G. & Penc, K. Cyclic exchange, isolated states, and spinon deconfinement in an XXZ Heisenberg model on the checkerboard lattice. Phys. Rev. B 69, 220403(R) (2004). URL https://link.aps.org/doi/10.1103/PhysRevB.69.220403.
- Haah, J. Local stabilizer codes in three dimensions without string logical operators. *Phys. Rev. A* 83, 042330 (2011). URL https://link.aps.org/doi/10.1103/PhysRevA.83. 042330.
- Vijay, S., Haah, J. & Fu, L. A new kind of topological quantum order: A dimensional hierarchy of quasi-particles built from stationary excitations. *Phys. Rev. B* 92, 235136 (2015). URL https://link.aps.org/doi/10.1103/PhysRevB.92.235136.
- Vijay, S., Haah, J. & Fu, L. Fracton topological order, generalized lattice gauge theory, and duality. *Phys. Rev.* B 94, 235157 (2016). URL https://link.aps.org/doi/ 10.1103/PhysRevB.94.235157.
- Bulmash, D. & Barkeshli, M. Higgs mechanism in higher-rank symmetric U(1) gauge theories. *Phys. Rev. B* 97, 235112 (2018). URL https://link.aps.org/doi/10.1103/PhysRevB.97.235112.
- Ma, H., Hermele, M. & Chen, X. Fracton topological order from the Higgs and partial-confinement mechanisms of rank-two gauge theory. *Phys. Rev. B* 98, 035111 (2018).

- Nandkishore, R. M. & Hermele, M. Fractons. Annual Review of Condensed Matter Physics 10, 295-313 (2019). URL https://doi.org/10.1146/ annurev-conmatphys-031218-013604.
- ³⁷ Slagle, K. & Kim, Y. B. Fracton topological order from nearest-neighbor two-spin interactions and dualities. *Phys. Rev. B* **96**, 165106 (2017). URL https://link.aps.org/doi/10.1103/PhysRevB.96.165106.
- ³⁸ Halász, G. B., Hsieh, T. H. & Balents, L. Fracton Topological Phases from Strongly Coupled Spin Chains. *Phys. Rev. Lett.* **119**, 257202 (2017). URL https://link.aps.org/doi/10.1103/PhysRevLett.119.257202.
- ³⁹ Schmitz, A. T., Ma, H., Nandkishore, R. M. & Parameswaran, S. A. Recoverable information and emergent conservation laws in fracton stabilizer codes. *Phys. Rev. B* 97, 134426 (2018). URL https://link.aps.org/doi/10.1103/PhysRevB.97.134426.
- ⁴⁰ Kubica, A. & Yoshida, B. Ungauging quantum errorcorrecting codes (arXiv:1805.01836). URL https:// arxiv.org/abs/1805.01836.
- ⁴¹ Benton, O., Jaubert, L. D. C., Yan, H. & Shannon, N. A spin-liquid with pinch-line singularities on the pyrochlore lattice. *Nature Communications* 7, 11572 (2016).
- ⁴² Pretko, M. Emergent gravity of fractons: Mach's principle revisited. *Phys. Rev. D* **96**, 024051 (2017). URL https: //link.aps.org/doi/10.1103/PhysRevD.96.024051.
- ⁴³ Yan, H. Hyperbolic fracton model, subsystem symmetry, and holography. *Phys. Rev. B* **99**, 155126 (2019). URL https://link.aps.org/doi/10.1103/PhysRevB.99. 155126.
- ⁴⁴ Pretko, M. & Radzihovsky, L. Fracton-Elasticity Duality. Phys. Rev. Lett. 120, 195301 (2018). URL https://link.aps.org/doi/10.1103/PhysRevLett.120.195301.
- Gromov, A. Chiral Topological Elasticity and Fracton Order. Phys. Rev. Lett. 122, 076403 (2019). URL https://link.aps.org/doi/10.1103/PhysRevLett.122.076403.
- ⁴⁶ You, Y., Bibo, J., Pollmann, F. & Hughes, T. L. Fracton Critical Point in Higher-Order Topological Phase Transition (2020).
- ⁴⁷ Zhou, Z., Zhang, X.-F., Pollmann, F. & You, Y. Fractal Quantum Phase Transitions: Critical Phenomena Beyond Renormalization (2021).
- ⁴⁸ You, Y., Burnell, F. J. & Hughes, T. L. Multipolar topological field theories: Bridging higher order topological insulators and fractons. *Phys. Rev. B* 103, 245128 (2021). URL https://link.aps.org/doi/10.1103/PhysRevB.103.245128.
- ⁴⁹ Xu, C. & Hořava, P. Emergent gravity at a Lifshitz point from a Bose liquid on the lattice. *Phys. Rev. D* 81, 104033 (2010). URL https://link.aps.org/doi/10.1103/PhysRevD.81.104033.
- Xu, C. & Fisher, M. P. A. Bond algebraic liquid phase in strongly correlated multiflavor cold atom systems. *Phys. Rev. B* **75**, 104428 (2007). URL https://link.aps.org/doi/10.1103/PhysRevB.75.104428.
- ⁵¹ Halász, G. B., Hsieh, T. H. & Balents, L. Fracton Topological Phases from Strongly Coupled Spin Chains. *Phys. Rev. Lett.* **119**, 257202 (2017). URL https://link.aps.org/doi/10.1103/PhysRevLett.119.257202.
- ⁵² You, Y. & von Oppen, F. Building fracton phases by Majorana manipulation. *Phys. Rev. Research* 1, 013011 (2019). URL https://link.aps.org/doi/10. 1103/PhysRevResearch.1.013011.
- ⁵³ Cowley, R. A. Acoustic phonon instabilities and structural

- phase transitions. *Phys. Rev. B* **13**, 4877-4885 (1976). URL https://link.aps.org/doi/10.1103/PhysRevB.13.4877
- ⁵⁴ Karahasanovic, U. & Schmalian, J. Elastic coupling and spin-driven nematicity in iron-based superconductors. *Phys. Rev. B* **93**, 064520 (2016). URL https://link.aps. org/doi/10.1103/PhysRevB.93.064520.
- Paul, I. & Garst, M. Lattice Effects on Nematic Quantum Criticality in Metals. Phys. Rev. Lett. 118, 227601 (2017). URL https://link.aps.org/doi/10.1103/PhysRevLett. 118.227601.
- ⁵⁶ de Carvalho, V. S. & Fernandes, R. M. Resistivity near a nematic quantum critical point: Impact of acoustic phonons. *Phys. Rev. B* **100**, 115103 (2019). URL https: //link.aps.org/doi/10.1103/PhysRevB.100.115103.
- Fernandes, R. M. & Venderbos, J. W. F. Nematicity with a twist: Rotational symmetry breaking in a moiré superlattice. *Science Advances* 6, eaba8834 (2020). URL https://doi.org/10.1126/sciadv.aba8834.
- Frem, A., Vijay, S., Chou, Y.-Z., Pretko, M. & Nand-kishore, R. M. Pinch point singularities of tensor spin liquids. *Phys. Rev. B* 98, 165140 (2018). URL https://link.aps.org/doi/10.1103/PhysRevB.98.165140.
- Yan, H., Benton, O., Jaubert, L. D. C. & Shannon, N. Rank-2 U(1) Spin Liquid on the Breathing Pyrochlore Lattice. Phys. Rev. Lett. 124, 127203 (2020). URL https://link.aps.org/doi/10.1103/PhysRevLett.124.127203.
- ⁶⁰ Benton, O. & Moessner, R. Topological Route to New and Unusual Coulomb Spin Liquids (2021).
- ⁶¹ Pomeranchuk, I. I. On the stability of a Fermi liquid. Zh. Eksp. Teor. Fiz. 35, 524 (1958). [Sov. Phys. JETP 8, 361 (1958)].
- Grimm, R., Weidemüller, M. & Ovchinnikov, Y. B. Optical Dipole Traps for Neutral Atoms. In Advances In Atomic, Molecular, and Optical Physics, 95–170 (Elsevier, 2000). URL https://doi.org/10.1016/s1049-250x(08) 60186-x.
- ⁶³ Bloch, I. Ultracold quantum gases in optical lattices. Nature Physics 1, 23–30 (2005). URL https://doi.org/10.1038/nphys138.
- ⁵⁴ Greiner, M., Mandel, O., Esslinger, T., Hänsch, T. W. & Bloch, I. Quantum phase transition from a superfluid to a Mott insulator in a gas of ultracold atoms. *Nature* 415, 39–44 (2002). URL https://doi.org/10.1038/415039a.
- ⁶⁵ Bakr, W. S., Gillen, J. I., Peng, A., Fölling, S. & Greiner, M. A quantum gas microscope for detecting single atoms in a Hubbard-regime optical lattice. *Nature* 462, 74–77 (2009). URL https://doi.org/10.1038/nature08482.
- ⁶⁶ Yang, B. et al. Cooling and entangling ultracold atoms in optical lattices. Science 369, 550-553 (2020). URL https://doi.org/10.1126/science.aaz6801.
- ⁶⁷ MacDonald, M. P., Spalding, G. C. & Dholakia, K. Microfluidic sorting in an optical lattice. *Nature* 426, 421–424 (2003). URL https://doi.org/10.1038/nature02144.
- ⁶⁸ Bloch, I., Dalibard, J. & Zwerger, W. Many-body physics with ultracold gases. Rev. Mod. Phys. 80, 885– 964 (2008). URL https://link.aps.org/doi/10.1103/ RevModPhys.80.885.
- ⁶⁹ Eckardt, A. Colloquium: Atomic quantum gases in periodically driven optical lattices. Rev. Mod. Phys. 89, 011004 (2017). URL https://link.aps.org/doi/10.1103/RevModPhys.89.011004.
- Oganesyan, V., Kivelson, S. A. & Fradkin, E. Quantum theory of a nematic Fermi fluid. Phys. Rev. B

 $\bf 64,\,195109~(2001).~URL~https://link.aps.org/doi/10. 1103/PhysRevB.64.195109.$

⁷¹ Isakov, S. V., Gregor, K., Moessner, R. & Sondhi, S. L. Dipolar Spin Correlations in Classical Pyrochlore Magnets. *Phys. Rev. Lett.* **93**, 167204 (2004). URL https://link.aps.org/doi/10.1103/PhysRevLett.93.167204.

I. BRIEF REVIEW OF RANK-2 U(1) GAUGE THEORY

We start by briefly reviewing a version of rank-2 U(1) gauge theory, which is to be realized in the models we propose in this paper.

As its name suggested, the R2–U1 gauge theory uses rank–2 tensors E_{ij} and A_{ij} as its electric and gauge field instead of vectors. More specifically, the tensor field is symmetric,

$$E_{ij} = E_{ji} , A_{ij} = A_{ji} .$$
 (24)

The charge is a vector defined as

$$\rho_i = \partial^k E_{ki} \ . \tag{25}$$

The low-energy sector of the theory has to be charge-free,

$$\partial^k E_{ki} = 0, (26)$$

which dictates the form of the gauge invariance condition

$$A_{ij} \to A_{ij} + \partial_i \lambda_j + \partial_i \lambda_j$$
 (27)

The magnetic field is the simplest object that is gauge-invariant,

$$B_{ij} = \epsilon_{iab} \epsilon_{jcd} \partial^a \partial^c A^{bd}. \tag{28}$$

One can now write down the Hamiltonian for the R2-U1 gauge theory as

$$\mathcal{H}_{\text{R2-U1}} = U \partial^k E_{ki} \partial^l E_{li} + E_{ij} E_{ij} + B_{ij} B_{ij}$$
$$= U \boldsymbol{\rho}^2 + \boldsymbol{E}^2 + \boldsymbol{B}^2$$
(29)

Here we assumed the Einstein's summation rule while not caring about the super- and sub-scripts.

Our aim in this paper is to find out a general, and experimentally realistic routes to realize the classical part of this Hamiltonian

$$\mathcal{H}_{\text{R2-U1-cl}} = U\boldsymbol{\rho}^2 + \boldsymbol{E}^2. \tag{30}$$

The quantum dynamics, i.e. the B^2 term, is also possible to realize, but is highly dependent on the specific set up of the physical system. It will not be a focus of this paper.